Journal of Hazardous Materials 176 (2010) 199–206

Contents lists available at ScienceDirect

Journal of Hazardous Materials

journal homepage: www.elsevier.com/locate/jhazmat

Trajectory measurements of a wall jet impinging onto a forward facing step entering a cross-flow

D.C. Langer, B.A. Fleck*, D.J. Wilson

Department of Mechanical Engineering, University of Alberta, Edmonton, Alberta, Canada T6G 2G8

ARTICLE INFO

Article history:
Received 27 May 2009
Received in revised form
10 September 2009
Accepted 3 November 2009
Available online 11 December 2009

Keywords:
Plume-trajectory
Impingement
Dispersion
Jet
Cross-flow

ABSTRACT

This study examines a horizontal wall jet impinging onto a forward facing step in a cross-flow. Planar laser induced fluorescence (PLIF) experiments in a water channel indicate that the wall-jet flow after impinging onto the step, becomes a vertical jet with an elliptical cross section. Experiments indicate that the jet trajectory scales with the perimeter of the elliptical jet issuing vertically into the cross-flow. The trajectory consists of three regions: the near-field region which is well described by a power law with an exponent of 1/2, the mid-field region where the jet is fully bent over which is described by a power law with an exponent of 1/3, and a far-field region where the jet is dominated by the cross-flow. This paper provides a prediction of the plume behaviour based on the geometric and initial conditions of the jet (diameter, step height, distance from jet to step, and velocity ratio) alone. The Briggs entrainment model for a round jet was also used to predict the trajectories of the jet in the cross-flow. It was found that the entrainment coefficients, α and β, for the elliptical jet case had average values of 0.15 and 0.58 respectively.

1. Introduction

This study examines the flow field which occurs when a wall jet impinges normally onto a forward facing step and is then deflected into a cross-flow. This geometry has not been closely examined and may have applications in mixing and dispersion studies. The primary motivation for studying this geometry is that most pipelines are buried and ruptures produce jets that strike the side of the resulting crater and are deflected to the vertical then bent over by the wind [1]. Planar laser induced fluorescence (PLIF) measurements were used for both flow visualization and to measure the concentration profiles within the jet. Two characteristics of the flow were measured: the shape of the vertically deflected jet above the step and the trajectory of the jet in the cross-flow. The first stage of this investigation was to characterize the vertical jet [2], this work indicated that the aspect ratio (S) and perimeter (P) of the vertical jet entering the cross-flow (based on the 70% concentration contour) can be predicted by the empirical Eqs. (1) and (2) respectively.

$$S = 8.38(HL_0)^{0.3}R^{0.4} \tag{1}$$

$$\frac{P}{d} = 1.84R^{0.2}\left(\frac{HL_0}{d^2}\right)^{1/2} - 5.79 \tag{2}$$

In these equations, the geometric and velocity terms defining the flow are defined as: the step height (H), the distance from a point source to the step (L_0), and the ratio of the jet velocity to the cross-flow velocity (R). Though the proper scaling parameter for this flow is the jet:cross-flow momentum ratio, in this work the density is uniform so this ratio is equal to R^2.

Given this information, the shape of the jet entering into the cross-flow is fully defined as a high-aspect ratio ellipse, with a major axis perpendicular to the cross-flow, and a minor axis in the direction of the cross-flow velocity. The aim of this study is to produce a predictive model of the jet centerline trajectory through the cross-flow based on these parameters, which can be used to aid in pollution dispersion studies.

The jet in cross-flow has received significant research attention in the past due to its importance in pollutant dispersion and fuel injection. Though scaling methods for round jets in cross-flow have been discussed in detail [3–7], more recently, the trajectories of elliptic jets in cross-flow have been studied by New et al. [8,9]. The elliptical jet in cross-flow was found to be strongly dependent on the jet exit geometry and could be scaled with the jet to cross-flow velocity ratio R multiplied by the hydraulic diameter of the jet [10]. However, due to "the unique flow dynamics of elliptic vortex loops" the trajectories may not collapse to a single curve as well as round jets in cross-flow [10]. Since the flow parameters in the present study generate jets with high-aspect ratios (>10), they may bear some similarity to plane jets in cross-flow as studied by Kalita et al. [11]. Because of the large variation in the shape and size of the jet

* Corresponding author. Tel.: +1 780 492 6773; fax: +1 780 492 2200.
E-mail address: brian.fleck@ualberta.ca (B.A. Fleck).

0304-3894/$ – see front matter © 2009 Elsevier B.V. All rights reserved.
doi:10.1016/j.jhazmat.2009.11.013

Nomenclature

A	area of jet
B_1	$x^{1/2}$ power law fit coefficient
B_2	$x^{1/3}$ power law fit coefficient
C_D	drag coefficient
S	aspect ratio of elliptical jet
d	diameter of initial round jet
D	minor axis of the elliptical cross section
h	height above step
H	step height
ℓ_m	momentum length scale
L	distance from jet to step
L_0	distance from an equivalent point source to step
P	perimeter of elliptical jet
R	ratio of the mean velocity of the jet exiting the pipe compared with the mean cross-flow velocity
R^*	ratio of the calculated velocity of the vertical jet entering the cross-flow to the local cross-flow velocity ratio at the top of the step
V_∞	cross-flow velocity
V	jet velocity
w_0	velocity of vertical jet emitted into cross-flow
x	distance from the vertical jet source
z	height from the floor of the waterchannel

Greek letters

α	entrainment coefficient with a theoretical value of 0.11
β	entrainment coefficient with a theoretical value of 0.6
β_e	elliptical entrainment coefficient
ρ	density

depending on the various inlet parameters, it may be impossible to collapse the trajectories onto a single line.

It was shown analytically and experimentally [12,13] that the round jet in cross-flow produced by an elevated stack has two distinct regions: the jet dominated region, and the bent-over plume region. They showed that in the jet dominated region the trajectory could be modeled analytically as a power law relating the height to the distance from the stack with an exponent of 1/2. After the jet had entrained sufficient cross-flowing fluid the cross-flow momentum was assumed to dominate the jet's behaviour, and in this fully bent-over region, a power law relation with an exponent of 1/3 is predicted in the analytical solution. In their experimental studies the jet dominated region was found to be very small, and present only very near to the source. In both cases, the jet to cross-flow velocity ratio significantly effected the jet trajectory and was used to normalize the data (along with the radius of the stack) and produce the power law relationships. Although the elliptical jet has quite different properties, intuitively these two regions should still exist. Initially the flow is dominated by the jet's momentum, and then at some point, the entrained cross-flowing fluid would dominate the momentum of the jet. The experimental data and predictions will be compared with the analytical model of Briggs [12] to determine if a round-jet model can be used to predict the trajectory of the elliptical jet in cross-flow.

2. Experimental method

Experiments were performed in the recirculating water channel facility at the University of Alberta which has been used extensively for jet and mixing studies [14–17]. The more recent study by the current authors [2] operated under similar conditions, though the cited work was both numerical and experimental and effectively determined the inlet conditions for the current work.

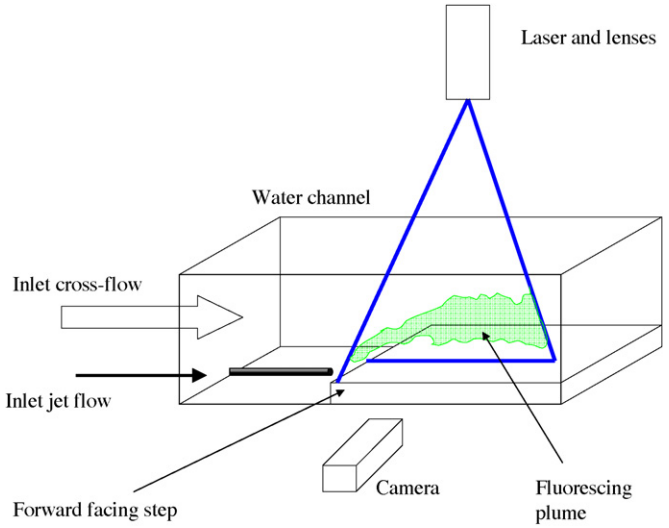

Fig. 1. Isometric schematic of the test section showing laser sheet optics, water channel, inlet flows and forward facing stem.

The experimental apparatus is shown schematically in Figs. 1 and 2. The system consists of a 5.24 m long rectangular channel with a cross section measuring 47 cm ×68 cm, with a water depth of 40 cm. The cross-flow was varied from 0.041 m/s to 0.081 m/s, producing Reynolds numbers (based on hydraulic diameter) ranging from 2×10^4 to 4×10^4. A turbulent boundary layer shear flow was developed in the channel using a grid composed of square aluminum tubes, a sawtooth trip fence, and roughness elements composed of a 1.27 mm diamond shaped steel mesh attached to acrylic panels on the bottom of the water channel. The shear flow used was measured by [14] and found to produce conditions similar to the atmospheric boundary layer.

The dyed jet was fed from a 1 m long pipe, with 8.75 mm ID running along the floor of the water channel midway between the side walls and parallel to the cross-flow. Upstream of the outlet an orifice turbulence generator ensured fully developed turbulent flow. Dyed water of equal temperature to the cross-flow was injected through the tube from a constant pressure vessel, ensuring

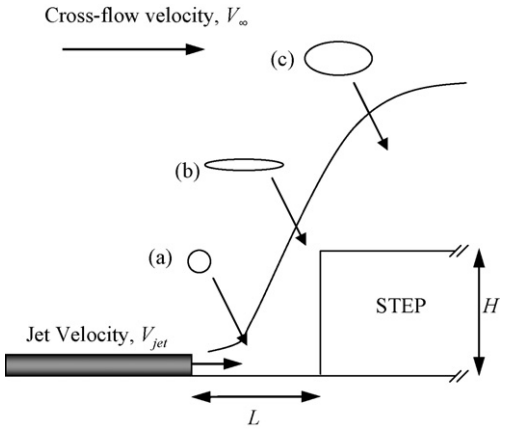

Fig. 2. Schematic of the test section. The step height (H), the effective distance (L) and the velocity ratio ($R = V_{jet}/V_\infty$) were varied for the parametric study. The shape of the cross section perpendicular to the direction of the jet is shown at three locations: the pipe exit (a), the top of the step (b), and downstream of the step (c). The round jet flattens at the step (b) and forms a high-aspect ratio ellipse which then 'rolls-up' to become more circular.

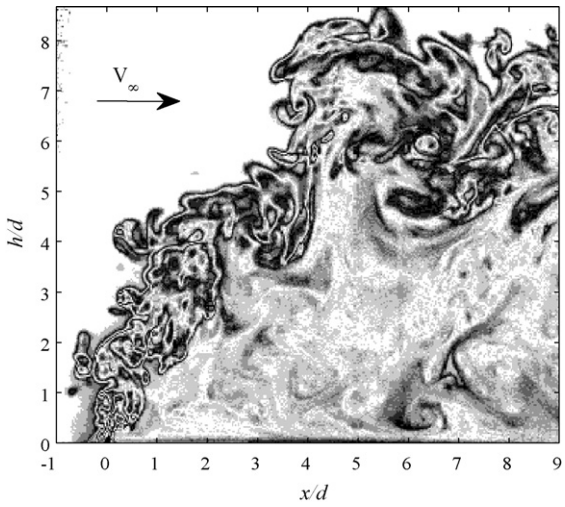

Fig. 3. Single jet image used for trajectory measurements. The concentration profile along the jet centerline is represented by a sawtooth function to emphasize the flow structures. The axes show the height above the step (h) against the distance from the step (x) both normalized with the initial jet diameter (d).

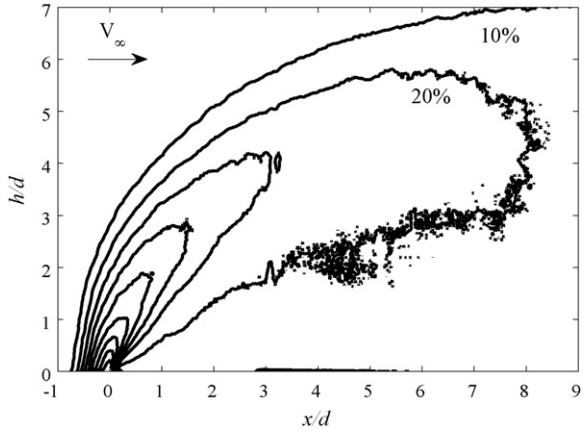

Fig. 4. Contour plot of the concentration of an averaged jet used for trajectory measurements. Contours vary from 10 to 90% of the maximum jet concentration. Axes represent the height above the step (h) versus the horizontal distance from the step (x) both normalized with the initial jet diameter (d).

constant flow rate. The velocity of the jet was controlled using a needle valve and a rotameter giving average jet velocities of 0.47, 0.78, and 1.10 m/s. This corresponded to pipe Reynolds numbers based on diameter of 4.1×10^3, 7.0×10^3, and 9.6×10^3.

The forward facing step traversed the entire water channel and was perpendicular to the cross-flow. Three step heights were used: 2.54, 3.81 and 5.08 cm. The jet outlet was located 5d, 9d and 15d from the step (43.75, 78.75 and 131.25 mm).

Images were taken to determine the trajectory of the jet after it deflected over the step. These measurements were taken with a vertical laser sheet located at the center of the jet. The measurement system was composed of a 4 W Coherent Innova 70 Argon-Ion laser, steering optics, a Powell lens, and a 12-bit Cooke SensiCam CCD camera. The laser was run in single line mode, producing a single beam at 488 nm, with a rated power of 2.1 W. The beam was passed through a focusing lens, decreasing the thickness of the laser sheet at the center of the water channel to approximately 1 mm. It was then steered by two mirrors into a 30° Powell lens [18]. The laser sheet was used to illuminate Fluorescein Sodium Salt ($C_{20}H_{10}Na_2O_5$) which was pre-mixed in the jet tank at a concentration of 0.2 mg/L. It was stated by Walker [19] that the absorption peak for this dye is approximately 488 nm and the emission peak is at 515 nm. A number 12 Kodak *wratten* gelatin filter was placed in front of the camera to effectively attenuate the laser sheet and reflected laser light from the recorded images. The filter was rated to have zero transmittance at 488 nm and approximately 25% transmittance at 515 nm. The camera was oriented perpendicular to the laser sheet and focused using a 75 mm Cosmicar TV Zoom Lens.

Calibration was required to remove the effects of the non-uniformity of the laser sheet's light intensity, which were caused by the spreading of the laser, the profile produced by the Powell lens, and the operating mode of the laser. The non-uniformities in the light sheet and camera array sensitivity were factored into the daily calibration using a method similar to that of Hilderman and Wilson [14,15] but assuming a linear concentration–fluorescence correlation [19].

Jet trajectories were measured using the PLIF system with the laser sheet aligned parallel to the jet flow and perpendicular to the floor of the water channel. Measurements were taken from the impingement point to approximately 8d downstream of the step. Instantaneous images had exposure times of 10 ms; an example of one is shown in Fig. 3. The averaged images were found by obtaining an arithmetic mean of 500 corrected instantaneous images obtained over 36 seconds. The resolution of the single images was 0.27 mm/pixel. A contour plot showing the concentration contours for an averaged image is shown in Fig. 4. The jet trajectory was defined as the location of the maximum scalar concentration [5]. Power law curves were fit to the maximum scalar data to represent the jet trajectory.

3. Experimental results

The jet in cross-flow was studied for a range of step heights, distances from the jet to the step, and velocity ratios. It was found that in all cases, the behaviour of the plume could be scaled with the perimeter of the jet exiting the step (which is proportional to an effective diameter). The use of P scaling showed three consistent regions in the jet: the near-field, the bent-over, and the far-field regions. Examples of these fits for a single jet trajectory are shown in Fig. 5.

It was found for all of the experiments that in the near-field region from $0 < x/P < 0.12$ the jet followed Eq. (3). This is consistent with Weil [13] who explains that in this region "the plume is dominated by its initial mass and momentum fluxes." Some exam-

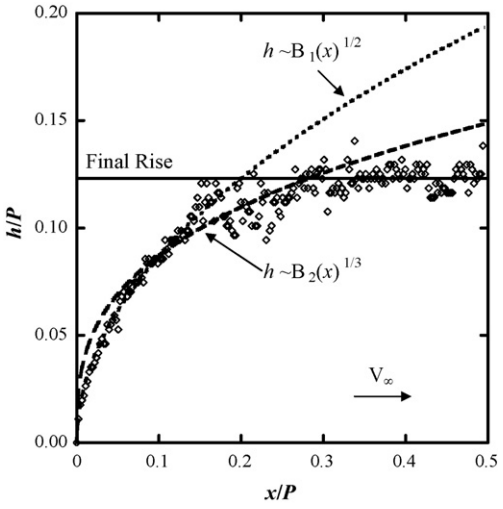

Fig. 5. Curve fits for a single jet trajectory measurement. The $h \backsim x^{1/2}$ fit is valid for $0 < x/P < 0.12$, the $h \backsim x^{1/3}$ fit is valid for $0.12 < x/P < 0.25$. The final rise is also approximated.

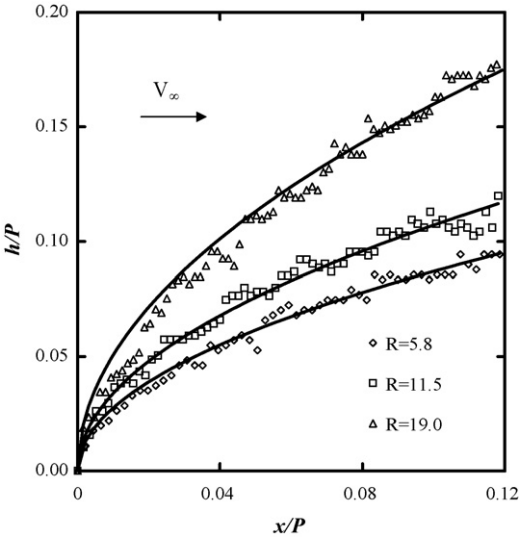

Fig. 6. Curve fits for the $h \backsim (B_1 x)^{1/2}$ power law relationship used to determine the constant B_1 fitted for three velocity ratios within $0 < x/P < 0.12$. These tests used a single step height and distance from the step. Jet penetration increases significantly with increasing jet to cross-flow velocity ratio.

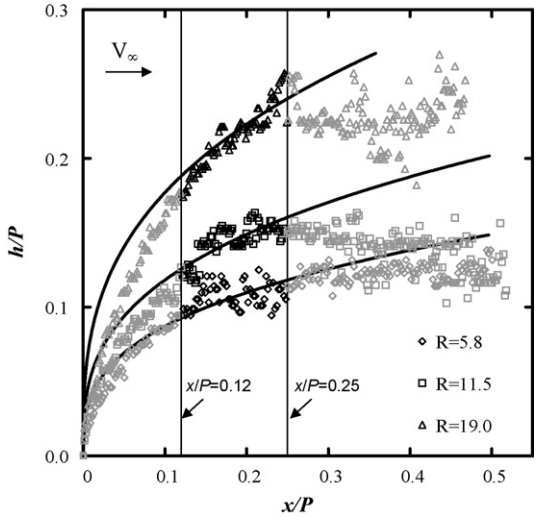

Fig. 8. Determination of B_1 from $h \backsim (B_1 x)^{1/2}$ in terms of the velocity ratio R, the step height H, the jet diameter d and the effective distance to the step L_0.

ples of the curve fits for this region are shown in Fig. 6. From this figure it can be seen that there is a strong correlation between the jet velocity ratio and the penetration of the jet into the cross-flow. The penetration is also affected by the geometric conditions of the impingement region (H and L) studied earlier [2]. It was found that increasing H and L both increase the spreading of the jet before it enters the cross-flow, which creates more surface area for entrainment of cross-flowing fluid and increases the drag force acting on the jet, decreasing its momentum. The effect of this momentum loss on Eq. (3) is a decrease in the coefficient B_1. An experimental correlation for B_1 is given in Eq. (4) and shown in Fig. 8. It should be noted that in Eq. (4) the initial jet diameter d is used to non-dimensionalize the height and length terms. This is used as a somewhat arbitrary length scale, as only one diameter was tested in these experiments. It is possible that another length-scale related to the initial turbulence or some sort of friction factor would be more appropriate for this correlation. The initial jet diameter is, however, quite commonly used in the literature for round jets in cross-flow as a scaling factor. Further research may find it to be a reasonable length scale. Despite the use of the jet diameter, Eq. (4) provides a good fit to the data shown in Fig. 8, and provides a prediction of the measured coefficient with a maximum deviation of 25%. Fig. 9

$$\frac{h}{P} = B_1 \left(\frac{x}{P}\right)^{1/2} \tag{3}$$

$$B_1 = 0.42 \left[R\left(\frac{d}{H}\right)\right]^{1/2} \left(\frac{d}{L_0}\right)^{1/4} \tag{4}$$

The bent-over region falls within $0.12 < x/P < 0.25$. Within this region, the one-third power law fit (given in Eq. (5)) is used to characterize the jet's trajectory. This also matches the trajectory predictions of [12,13] in form, with different definitions of the entrainment coefficients. The experimental correlation for the coefficient B_2 is given by Eq. (6) and its fit is shown in Fig. 7. This function is again dependent on d for convenience only. In this region, according to [13], the jet is fully bent-over, and its trajectory is dominated

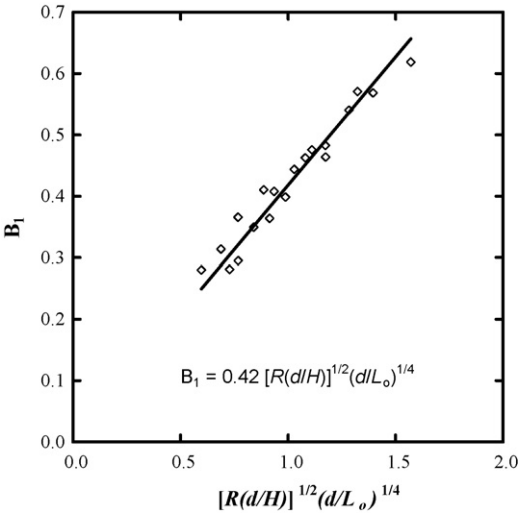

Fig. 7. Curve fits for the $h \backsim (B_2 x)^{1/3}$ power law relationship used to determine the constant B_2 fitted for three velocity ratios within $0.12 < x/P < 0.25$. These tests used a single step height and distance from the step. Jet penetration increases significantly with increasing jet to cross-flow velocity ratio. Further downstream than $x/P = 0.25$ the cross-flow momentum, and thus the trajectory bends down towards the floor of the channel for some cases.

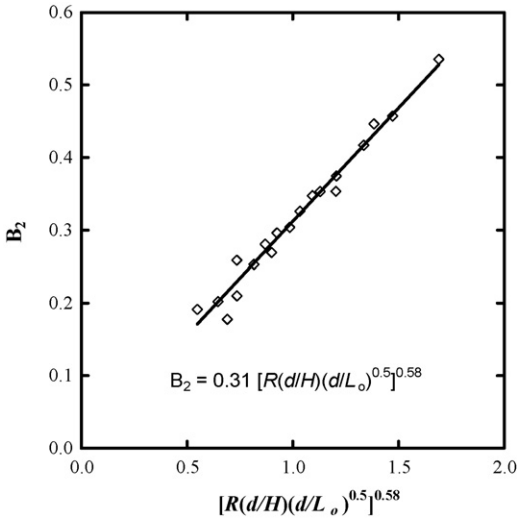

Fig. 9. Determination of B_2 from $h \backsim (B_2 x)^{1/3}$ in terms of the velocity ratio R, the step height H, the jet diameter d, and the effective distance to the step L_0.

by the cross-flowing fluid which it has entrained. The correlation defined in Eq. (6) was found to predict the measured fit coefficients with a maximum deviation of 34%. This provides a reasonable prediction, because in this location, low jet to cross-flow velocity ratios begin to appear more like the far-field region, as shown by the $R = 5.8$ data in Fig. 7. This causes the model to over-predict their rise.

$$\frac{h}{P} = B_2\left(\frac{x}{P}\right)^{1/3} \tag{5}$$

$$B_2 = 0.31\left[R\left(\frac{d}{H}\right)\left(\frac{d}{L_0}\right)^{0.5}\right]^{0.58} \tag{6}$$

The far-field region ($x/P > 0.25$) was found to be very erratic under the measurement conditions tested. This was most likely due to the effects of the walls, caused by the significant spreading of the jet in relation to the size of the water channel. It also appeared that the jet's behaviour was completely dominated by the momentum of the cross-flowing fluid which it had entrained. In some cases the jet stopped rising and began to fall (Fig. 7. This was due to the recirculation zone caused by the step [20]. Since the jet's initial vertical momentum was dominated by the momentum of the entrained cross-flowing fluid, the downward bending of the cross-stream caused the jet's trajectory to bend towards the floor. Thus, the final rise of the plume is not known for these experiments, and further experiments would be required to determine the exact location of the final rise region of the plume. The jet's final rise can be approximated by using Eq. (5) with $x/P = 0.25$.

4. Entrainment model

Existing analytical round jet entrainment models were tested to determine the accuracy of using these models for the case of the jet impinging onto the step. The analytical models presented by Briggs [12] and Weil [13] are given in Eqs. (8) and (9) which show the height of the jet (h) based on the distance from the jet's source (x). The relationship uses R^*, which is the velocity ratio comparing the vertical jet entering the cross-flow and the velocity of the cross-flow. They also define a momentum length scale, ℓ_m, which is given below in Eq. (7), which is dependent on the density ratio, the velocity ratio R^* and the radius of the initial round jet entering the cross-flow (r_0). The two coefficients, α and β were determined experimentally by Briggs [12] to be 0.11 and 0.6 respectively for round jets in cross-flow. These values will be compared with the experimental results presented here for the jet emerging vertically after impinging onto the step.

$$\ell_m = \left(\frac{\rho_0}{\rho_a}\right)^{1/2} R^* r_0 \tag{7}$$

$$\frac{h}{\ell_m} = \left(\frac{R^*}{\alpha R^* + \beta}\right)^{1/2}\left(\frac{x}{\ell_m}\right)^{1/2} \tag{8}$$

$$\frac{h}{\ell_m} = \left(\frac{3}{\beta^2}\right)^{1/3}\left(\frac{x}{\ell_m}\right)^{1/3} \tag{9}$$

Note that in these experiments, the density is uniform, so $\ell_m = R^* r_0$.

In order to use the round jet model to define the elliptical jet in cross-flow presented in this study, an equivalent value for each term is required. The two difficult parameters to determine are the velocity ratio (R^*) and the source radius (r_0). The velocity of the jet is determined by the use of conservation equations (mass flux and momentum flux given in Eqs. (10) and (11) which is derived by Langer [21]) and are dependent on the shape and cross-sectional areas of the vertical jets, as well as the losses present below the lip of the step.

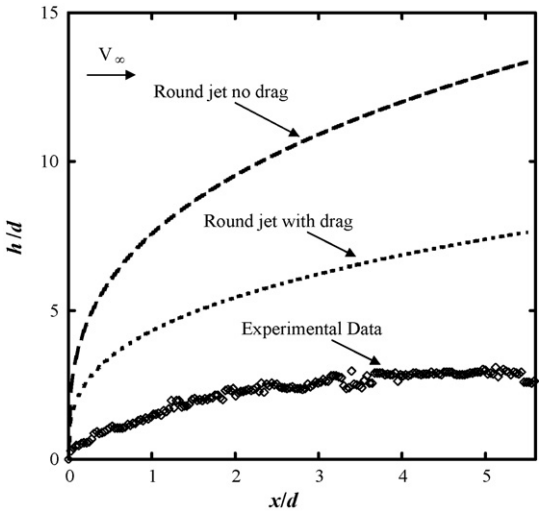

Fig. 10. Predicted jet trajectories assuming that the jet entering the cross-flow is circular. The first curve represents the case with no drag and no shape change. The second curve uses a round jet with a drag coefficient of 1.6 which was calculated from the measured elliptical jet's cross-sectional area. Both cases use an entrainment coefficient of β=0.6.

$$\rho_1 V_1 A_1 = \rho_2 V_2 A_2 \tag{10}$$

$$\rho_1 A_1 V_1^2 = \frac{1}{2} C_D \rho_1 A_1 V_1^2 + \rho_2 A_2 V_1^2 \tag{11}$$

The cross-flow velocity used was estimated for a location midway between the step and the maximum plume rise using the velocity profile measured by [14].

The source radius (r_0) is typically half of the thickness of the jet cross section. For a round jet this represents the radius of the jet, and for an elliptical jet it is half of the minor axis of the ellipse.

The simplest and most apparent model for this system would be to assume the horizontal jet was directed vertically without changing shape or losing momentum. In this case, the jet would have both the same speed and radius as the initial jet. This case is shown as the round jet with no drag in Fig. 10. From this it can be seen that the over-prediction of the rise is very significant and unrealistic. To improve the accuracy of this model, the cross-sectional

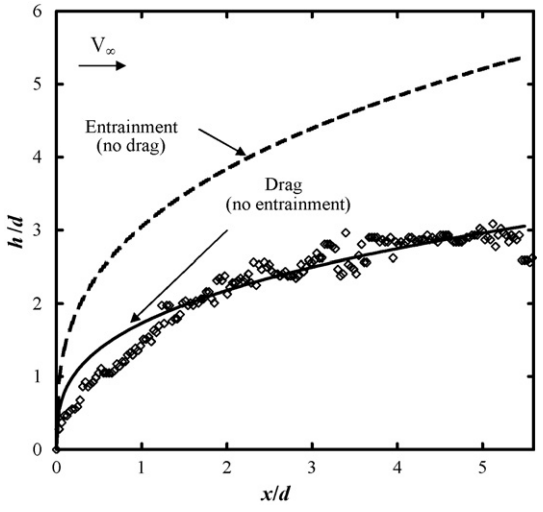

Fig. 11. Effect of the jet shape on its trajectory. The trajectories were calculated assuming the shape of the jet entering the cross-flow was round and elliptical. Both jets had the same area and their calculated drag coefficients were both 1.6.

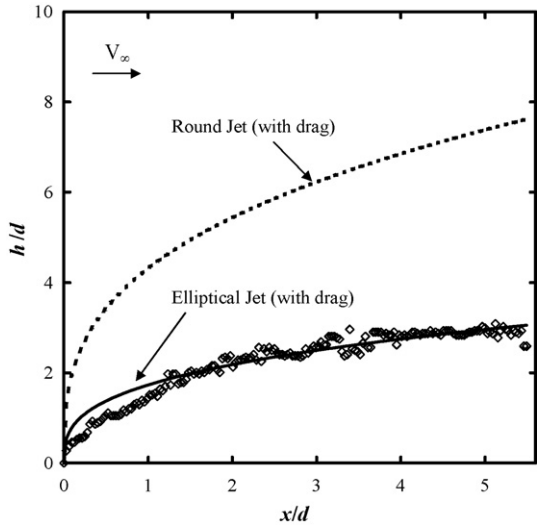

Fig. 12. Jet trajectories calculated assuming that the jet's trajectory is determined by drag and entrainment. Both trajectories assume an entrainment coefficient in the cross-flow of $\beta = 0.6$. The drag cases uses a calculated drag coefficient of 1.6.

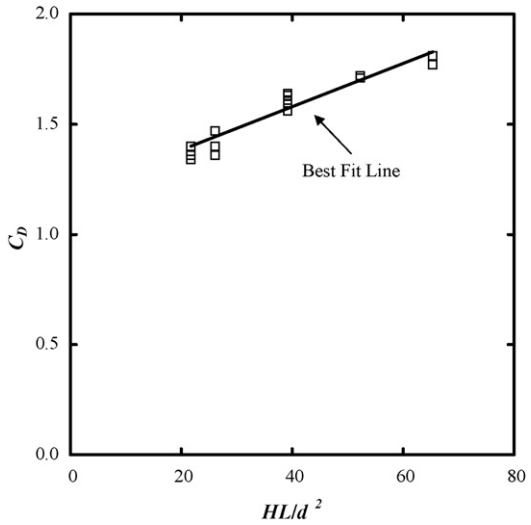

Fig. 14. Effect of the step position (L) and height (H) on the calculated drag coefficient. The increase in HL increases the surface area which the jet travels over before entering the cross-flow, increasing the momentum loss due to drag.

area of the vertical jet was set to match the area of the ellipse measured in [2]. For this case it is assumed that the change in shape is caused by drag losses which the jet experiences as it travels along the floor of the channel. The trajectory of this round jet (shown as round jet with drag) is shown in Fig. 10. The friction losses were found to have a drag coefficient of 1.6 for this case. From this it can be seen that simplifying the model to a round jet under-predicts the entrainment of cross-flowing fluid and leads to over-prediction of the maximum rise. To improve the accuracy of the model, it is apparent that the elliptical shape measured in [2] must be incorporated into the model. Fig. 11 shows a comparison of a round jet with an elliptical jet which both have the same cross-sectional area. In both cases the losses are due to a drag force with a coefficient of 1.6. The use of the elliptical cross-section significantly improves the fit of the model to the data.

It can be argued that as the wall jet travels along the floor and the fluid impinges onto the step, it entrains surrounding fluid. This entrainment explains both the spread and the change in the mean velocity of the jet. To determine the effect of this entrainment, the trajectory of this jet was determined by assuming that there was no drag force (so the momentum flux of the initial jet and the jet entering the cross-flow are equal), and the decrease in the mean jet velocity was caused by the addition of mass into the flow. Fig. 12 shows a comparison between the trajectory of the jet assuming entrainment with the trajectory assuming a drag coefficient of 1.6. In this case it is apparent that the use of a drag force explains the change in the jet's behaviour better than entrainment before the step. Fig. 13 shows the effect of the velocity ratio on the calculated drag coefficient, and shows that as expected, when the jet's Reynolds number increases the jet experiences less drag. The drag coefficient is more strongly influenced by the geometry of the step as shown in Fig. 14. This shows that the more the jet is in contact with the wall, the more drag acts on the jet. From this it appears that using the elliptical cross section, with r_0 defined as half of the minor axis of the ellipse, and assuming that the changes in jet shape and velocity before the top of the step are caused by drag forces lead to the most accurate prediction of the jet trajectory.

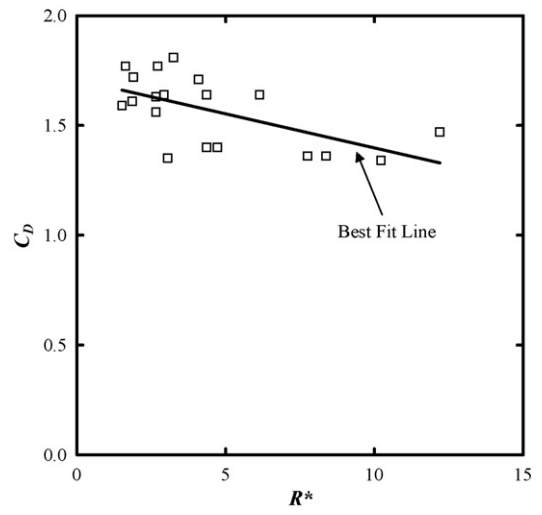

Fig. 13. Effect of the local velocity ratio (R^*) on the calculated drag coefficient (C_D). The trend is weak and may be due to scatter in the data. However, the drag coefficient decreases with Reynolds number as expected.

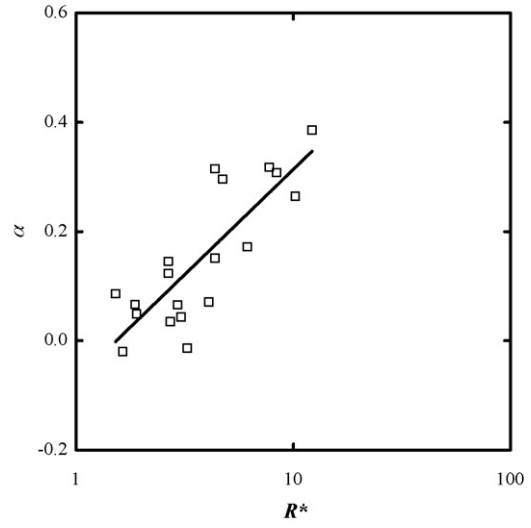

Fig. 15. Entrainment coefficient α given in Eq. (8) ($h \backsim x^{1/2}$) for the near-field region for the jet. The value presented in Weil [13] is constant with $\alpha = 0.11$. Here, the average is $\alpha = 0.15$ with a standard deviation of 0.13.

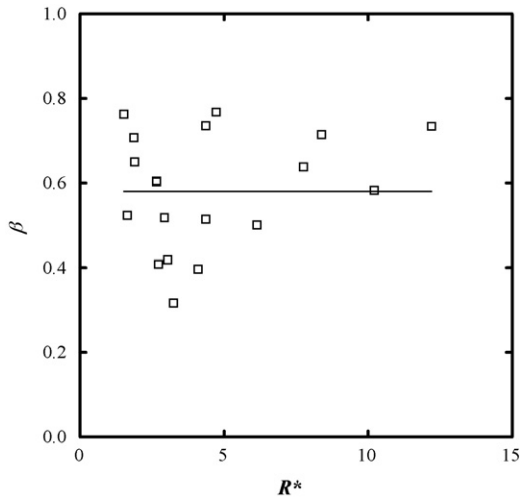

Fig. 16. Entrainment coefficient β for the fully bent-over region of the jet calculated using Eq. (9) ($h \backsim \beta^{-2/3}x^{1/3}$). The value given in Briggs [12] and Weil [13] is $\beta = 0.6$. Here the mean is $\beta = 0.58$ (shown with the horizontal line) with a standard deviation of 0.14.

After calculating the jet velocity entering the cross-flow the entrainment coefficients from Eqs. (8) and (9) were determined through the use of the empirical correlations given in Eqs. (3) and (5). This produced the relationship for β given in Eq. (12).

$$\beta = \left(\frac{3}{B_2}\right)^{1/2} R^* \left(\frac{D}{2P}\right) \tag{12}$$

Fig. 15 shows the dependence of α on the velocity ratio. The average value of α was found to be 0.15 with a standard deviation of 0.13, and it appears to have a slight dependence on R^*. However, with the large quantity of scatter, it is possible that the value approaches the average presented by [13] of $\alpha = 0.11$. From Fig. 16 it can be seen that the velocity ratio has little dependence on β. Due to the large scatter, the average value of β is recommended, which has a value of 0.58, with a standard deviation of 0.14. The average value presented by Briggs [12] is $\beta = 0.6$, which agrees with the value measured by these experiments. Fig. 17 gives the two curve fits using Eqs. (8) and (9) for a single jet trajectory image.

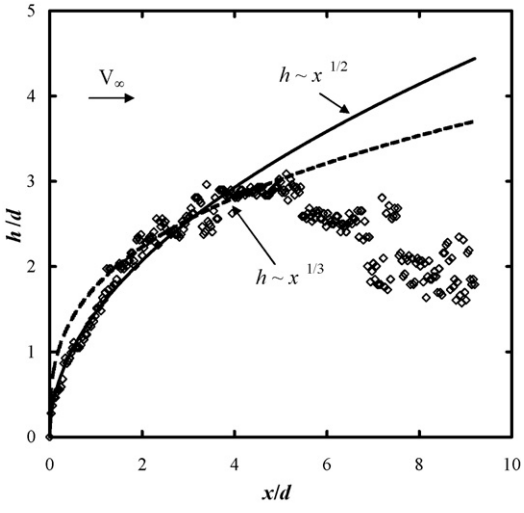

Fig. 17. Curve fits using the average values of $\alpha = 0.15$ and $\beta = 0.58$ for a single jet using $h \backsim (\alpha, \beta)\, x^{1/2}$ and $h \backsim \beta^{-2/3}x^{1/3}$. In the far-field region, the bending streamlines in the cross-flow due to the recirculation over the step [20] causes the jet to bend towards the floor of the channel.

This figure shows the accuracy of the trajectory predicted using the entrainment model. It shows a reasonable fit in the near-field and bent-over jet region, but in the far field it over-predicts the final plume rise.

5. Conclusions

This study has presented two methods of predicting the trajectory of an elliptical jet in cross-flow formed by a wall jet impinging onto a forward facing step. In both cases the flow contained three regions: a near-field region dominated by the initial jet momentum, the fully bent-over region where the cross-flowing fluid has been entrained, and the far-field region where the jet's rise has stopped. In the near-field region a power law fit with an exponent of 1/2 was found to best fit the trajectory data. In the fully bent-over region, the exponent to the power law was 1/3. This is consistent with the round jet in cross-flow analytical models given in [12,13]. In the far-field the jet stopped rising and in some cases fell below its maximum rise. This was most likely caused by wall effects and a recirculation zone over the step changing the velocity profile of the cross-flowing fluid. The two models presented varied significantly in their approach. The first model used experimental correlations relating the jet's inlet velocity ratio and the step's geometry to the experimental curve fit. The second model used a modified version of the analytical entrainment models presented by [12,13] for round jets. The entrainment coefficients for the round jets were found to be within one standard deviation of those calculated using the elliptical jet model. It was also determined that the spreading of the jet along the wall and during impingement was dominated by a drag force with an average drag coefficient of 1.6. Based on the scatter in the data it is recommended that the empirical correlations be used to predict the jet trajectories.

Acknowledgements

The work presented here was made possible by NSERC research grants to BAF and DJW, and an NSERC graduate scholarship to DCL.

References

[1] D.J. Wilson, The release and dispersion of gas from pipeline ruptures, Technical report, Alberta Environment, 1979.
[2] D.C. Langer, B.A. Fleck, D.J. Wilson, Measurements of a wall jet impinging onto a forward facing step, Journal of Fluids Engineering 131 (2009) 091103.
[3] J.E. Broadwell, R.E. Breidenthal, Structure and mixing of a transverse jet in incompressible flow, Journal of Fluid Mechanics 148 (1984) 405–412.
[4] A.R. Karagozian, An analytical model for the vorticity associated with a transverse jet, AIAA Journal 24 (1986) 429–436.
[5] S.H. Smith, M.G. Mungal, Mixing, structure and scaling of the jet in crossflow, Journal of Fluid Mechanics 357 (1998) 83–122.
[6] S. Muppidi, K. Mahesh, Study of trajectories of jets in crossflow using direct numerical simulations, Journal of Fluid Mechanics 530 (2005) 81–100.
[7] L.L. Yuan, R.L. Street, Trajectory and entrainment of a round jet in crossflow, Physics of Fluids 10 (9) (1998) 2323–2335.
[8] T.H. New, T.T. Lim, S.C. Luo, Elliptic jets in cross-flow, Journal of Fluid Mechanics 494 (2003) 119–140.
[9] T.H. New, T.T. Lim, S.C. Luo, A flow field study of an elliptic jet in cross flow using DPIV technique, Experiments in Fluids 36 (2004) 604–618.
[10] T.T. Lim, T.H. New, S.C. Luo, Scaling of trajectories of elliptic jets in crossflow, AIAA Journal 44 (12) (2006) 3157–3160.
[11] K. Kalita, A. Dewan, A.K. Dass, Prediction of turbulent plane jet in crossflow., Numerical Heat Transfer, Part A 41 (2002) 101–111.
[12] G.A. Briggs, Plume rise predictions, In: D.A. Haugen (Ed.), Lectures on Air Pollution and Environmental Impacts Analysis, American Meteorological Society, Boston, 1975, pp. 59–111.
[13] J.C. Weil, Plume rise, In: A. Venkatram, J.C. Wyngaard (Eds.), Lectures on Air Polultion Modelling, American Meteorological Society, 1988, pp. 119–162.
[14] T.L. Hilderman, D.J. Wilson, Predicting plume meandering and averaging time effects on mean and fluctuating concentrations in atmospheric dispersion simulated in a water channel, Boundary-Layer Meteorology 122 (2007) 535–575.

[15] T.L. Hilderman, D.J. Wilson, Effect of vertical wind shear on concentration fluctuation statistics in a point source plume, Boundary-Layer Meteorology 129 (2008) 65–97.
[16] K. Shahzad, B.A. Fleck, D.J. Wilson, Small scale modeling of vertical surface jets in cross-flow: Reynolds number and downwash effects, Journal of Fluids Engineering 129 (2007) 311–318.
[17] C.R. Johnston, D.J. Wilson, A vortex pair model for plume downwash into stack wakes, Atmospheric Environment 31 (1) (1997) 13–20.
[18] I. Powell, Design of a laser beam line expander, Applied Optics 26 (17) (1987) 3705–3709.
[19] D.A. Walker, A fluorescence technique for measurement of concentration in mixing liquids, Journal of Physics E: Scientific Instrumentation 20 (1987) 217–224.
[20] J.G. Barbosa-Saldana, N.K. Anand, Flow over a three-dimensional horizontal forward-facing step, Numerical Heat Transfer, Part A: Applications 53 (2008) 1–17.
[21] D.C. Langer, The impingement of a turbulent wall jet onto a forward facing vertical step, Master's thesis, University of Alberta, 2008.